

Magnetic fields in Bok globules: Multi-wavelength polarimetry as tracer across large spatial scales[★]

S. Jorquera¹ and G. H.-M. Bertrang¹

Universidad de Chile, Departamento de Astronomía, Casilla 36-D, Santiago, Chile
e-mail: sebastian.jorquera.c@ing.uchile.cl; astro@gesabertrang.com

July 22, 2022

ABSTRACT

Context. The role of magnetic fields in the process of star formation is a matter of continuous debate. Clear observational proof of the general influence of magnetic fields on the early phase of cloud collapse is still pending. First results on Bok globules with simple structures indicate dominant magnetic fields across large spatial scales (Bertrang et al. 2014).

Aims. The aim of this study is to test the magnetic field influence across Bok globules with more complex density structures.

Methods. We apply near-infrared polarimetry to trace the magnetic field structure on scales of $10^4 - 10^5$ au in selected Bok globules. The combination of these measurements with archival data in the optical and sub-mm wavelength range allows us to characterize the magnetic field on scales of $10^3 - 10^6$ au.

Results. We present polarimetric data in the near-infrared wavelength range for the three Bok globules CB34, CB56, and [OMK2002]18, combined with archival polarimetric data in the optical wavelength range for CB34 and CB56, and in the sub-millimeter wavelength range for CB34 and [OMK2002]18. We find a strong polarization signal ($P \geq 2\%$) in the near-infrared for all three globules. For CB34, we detect a connection between the structure on scales of $10^4 - 10^5$ au to $10^5 - 10^6$ au. For CB56, we trace aligned polarization vectors in both the near-infrared and optical data, suggesting a connection of the magnetic field structure across the whole globule. In the case of [OMK2002]18, we find ordered polarization structures on scales of $10^4 - 10^5$ au.

Conclusions. We find strongly aligned polarization vectors on large scales which indicate dominant magnetic fields across Bok globules of complex density structures.

Key words. Magnetic fields – Polarization – Stars: formation – Stars: low-mass – ISM: clouds – Instrumentation: polarimeters

1. Introduction

Magnetic fields have been discussed to play a significant role in the star formation process (e.g., Galli 2009; Federrath 2015; Lizano & Galli 2015), as they can influence the contraction timescale, the gas dust coupling, the shape of the cloud fragments, and they launch jets and outflows (e.g; McKee & Ostriker 2007). The structure of magnetic fields in the dusty envelopes around young stellar objects can be derived from the polarization of background starlight due to dichroic extinction and thermal emission by dust grains (Weintraub et al. 2000; Girtart et al. 2008). In the case of polarization due to thermal emission, the polarization direction is perpendicular to the magnetic field lines, as the dust grains get partially aligned to the magnetic field, with their major axes perpendicular to the magnetic field lines, projected onto the plane-of-sky (POS; e.g., Hoang et al. 2007; Lazarian 2007; Bertrang & Wolf 2017). The light of the background stars that runs through the star-forming region also becomes polarized due to dichroic absorption by the dust grains. In this case, the polarization direction directly traces the magnetic field lines, projected onto the POS (Weintraub et al. 2000).

The influence of magnetic fields on low-mass star formation is best verified when studied independently of other phenomena such as turbulence or stellar feedback. Bok globules (Bok & Reilly 1947) arise as the ideal candidates to study the

magnetic field influence on low-mass star forming regions. Bok globules are small, isolated, relative simple structured molecular clouds (e.g; Clemens et al. 1991), and are often associated with low-mass star formation (Clemens & Barvainis 1988; Yun & Clemens 1994; Launhardt & Henning 1997). Bok globules are in particular ideal environments to study the correlation between protostellar collapse, fragmentation, and magnetic fields, as these objects are less affected by large-scale turbulences and other nearby star-forming events.

The classical method to characterize magnetic fields is the linearly polarized dust emission and dichroic absorption. Thermal emission of the dust grains, observable in the submillimeter (sub-mm) wavelength range, traces the polarization of the densest, innermost part of the globule, due to the sensitivity of millimeter/sub-mm telescopes. The outer, less dense parts of the globule are traced by the polarization of background starlight due to dichroic absorption, observable in the near infrared (near-IR)/optical wavelength range. Thus, by applying multi-wavelength polarimetry, it is possible to trace the magnetic field on large scales across the globule. This approach has been used in previous studies (e.g., Henning et al. 2001; Bertrang et al. 2014; Chakraborty & Das 2016), indicating dominant magnetic fields in Bok globules of simple density structures. This motivated us to extend our study to Bok globules with more complex density structures.

[★] Based on observations made with an ESO telescope at the La Silla Observatory under programme ID 096.C-0115. (PI: G. H.-M. Bertrang)

Table 1. Polarization standard stars.

Instrument	Object	α_{2000} (hh:mm:ss.ss)	δ_{2000} (dd:mm:ss.ss)	Type	P (%)	γ ($^{\circ}$)	Filter	Ref.
SOFI/NTT	CMa R1 No.24	07:04:47.36	-10:56:17.44	polarized	2.1 ± 0.05	86 ± 1	J	1
	HD64299	07:52:25.51	-23:17:46.78	unpolarized	0.151 ± 0.032		B	2
	WD0310-688	03:10:31.02	-68:36:03.39	unpolarized	0.051 ± 0.09		V	3

References. (1) Whittet et al. (1992); (2) Turnshek et al. (1990); (3) Fossati et al. (2007).

2. Description of the sources

Our aim is to verify the large-scale magnetic field influence on low-mass star formation. As stated in Sect. 1, Bok globules are ideal candidates for this kind of study. Furthermore, we have to restrict us to globules with available archival sub-mm or optical polarization maps that trace the magnetic field structure at scales not observable in the near-IR wavelength range. We further aim at expanding our previous study of the magnetic field structure in low-mass star-forming regions (Bertrang et al. 2014) to more complex structured objects. We found that these criteria are satisfied by three Bok globules: CB34, CB56, and [OMK2002]18.

CB34 is a Bok globule located at a distance of ~ 1.5 kpc (Launhardt & Henning 1997). The inner region of the globule discloses three dense cores (C1, C2, C3), each extends by ~ 2.5 pc in diameter (Codella & Scappini 2003; Launhardt et al. 2010). Their masses are $52 M_{\odot}$ (C1), $94 M_{\odot}$ (C2), and $13 M_{\odot}$ (C3), respectively (Fig. 1; Codella & Scappini 2003). These cores exhibit ongoing star formation based on the presence of a water maser as well as several collimated outflows (Fig. 1; Gómez et al. 2006; Huard et al. 2000; Yun & Clemens 1994). The chemical age of the globule is estimated to be $>10^5$ yr (Launhardt et al. 2010), with the presence of a pre-main-sequence star with an age of $\sim 10^6$ yr located in the core C1 (Alves et al. 1997). This massive globule encloses within its center $(4.05 \times 2.25) \times 10^5$ au about $110 - 170 M_{\odot}$ (Launhardt et al. 2010; Codella & Scappini 2003; Launhardt et al. 1998).

CB56 is a compact, irregular shaped cloud with a major and minor axis of $4''.5$ and $2''.5$ respectively (Dutra & Bica 2002). Its major axis has a position angle of 170° with respect to the galactic plane. CB56 is associated with two infrared point sources (IRAS 07125-2503 and IRAS 07125-2507; Clemens & Barvainis 1988). The distance to CB56 has yet to be determined. The optical polarization signal of this globule is significantly stronger than the interstellar polarization in the optical wavelength range within 200 pc (Chakraborty et al. 2014, Gontcharov 2018, priv. comm.). Together with the strong near-IR polarization, this indicates that CB56 is located within a distance of 200 pc and the measured polarization signal is associated with CB56.

[OMK2002]18 is a low-mass star forming region at a distance of 140 pc (Maheswar et al. 2011). It consist of the two dense clouds [OMK2002]18a and [OMK2002]18b. Both clouds have a radius of $\sim 4.125 \times 10^3$ au and enclose masses of $2.3 M_{\odot}$ and $1.1 M_{\odot}$ respectively (Onishi et al. 2002). OMK[2002]18 is associated with one compact infrared source (IRAS 04191+1522; Onishi et al. 2002).

3. Observations

The observations were performed in the near-IR with the instrument Son OF ISAAC (SOFI) at the 3.58 m New Technology Telescope (NTT) from November 11th to 15th, 2015. SOFI/NTT is mounted at the Nasmyth A focus, equipped with a 1024×1024

Hawaii Rockwell array optimized for wavelengths of $1 - 2.5 \mu\text{m}$. In SOFI/NTT, a single Wollaston prism is used for polarization observations. In this observing mode, the polarized flux is measured simultaneously at two different angles that differ by 90° . To derive the linear polarization degree and orientation of an object, two observations must be performed at each pointing of the telescope with different orientations of the Wollaston prism, typically 0° and 45° . This is realized by a rotation of the complete instrument. To avoid overlapping between different polarization images an aperture mask of three alternating opaque and transmitting strips of about $40'' \times 300''$ for SOFI/NTT is used.

We carried out Js-band polarization observations of three fields of CB34 and [OMK2002]18ab as well as one field of CB56.

4. Data Reduction

For the data reduction, we apply an specialized pipeline created to work with polarization data obtained with SOFI/NTT (Bertrang et al. 2014). This pipeline performs bias correction, flat-fielding, and instrumental polarization extraction as well as the calculation of the Stokes parameters I , Q , and U via aperture photometry. Table 1 summarizes the information of polarized and unpolarized standard stars used to determine the instrumental polarization.

A correction factor for the Wollaston prism was computed for the reduction of the instrumental polarization (see Appendix). This correction factor was tested for the polarized standard star, and as a successful test, the polarization data obtained after bias correction corresponds well to literature values.

5. Polarization Maps

In this section, we present the polarization maps of the three Bok globules CB34, CB56, and OMK[2002]18. We compare our near-IR data to archival polarization data in the optical and sub-mm wavelength range. As stated in Sect. 1, the polarization at these different wavelength ranges arises from different sources: while the polarization in the sub-mm range arises from thermal emission, in the near-IR and the optical it is caused by dichroic absorption. Thus, the polarization of a dust grain observed in the sub-mm is oriented perpendicular to the polarization of the very same dust grain observed in the near-IR or optical.

For CB34, data from all of the three wavelength ranges is available. This enables an analysis over the whole range of scales in this globule, from its most dense center (sub-mm) towards the less dense outer envelope (near-IR, optical).

For CB56, the data set is restricted to archival data in the optical wavelength range (Paul et al. 2012; Chakraborty et al. 2014) in addition to the newly obtained near-IR data. However, those two wavelength ranges cover this object almost completely. For this comparison, we make use of the optical polarization data published in Chakraborty et al. (2014), given that it is the more comprehensive data set at this wavelength range.

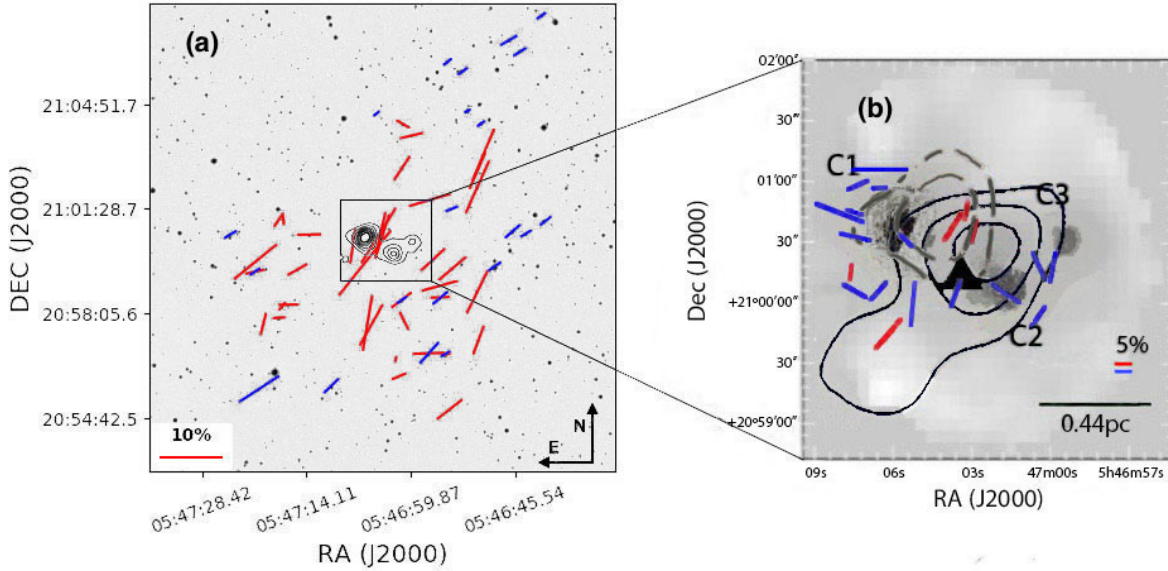


Fig. 1. (a) Near-IR polarization vectors (red) and optical polarization vectors (blue) are plotted over a $15' \times 15'$ R-Band DSS image of the field containing CB34. A 10% polarization vector is drawn as reference for both data sets into the lower left corner. Contours correspond to JCMT/SCUBA $850 \mu\text{m}$ dust continuum emissions from 0.1 to 0.7 Jy beam^{-1} , with intervals of 0.1 Jy beam^{-1} (Das et al. 2016). (b) Zoom into the dense center of CB34. The near-IR polarization vectors (red) and the archival sub-mm polarization vectors (blue) are plotted over the total continuum intensity map at $850 \mu\text{m}$ (Das et al. 2016). The sub-mm vectors are binned over a $10'' \times 10''$ grid. The solid (dashed) black (gray) contour lines correspond to blueshifted (redshifted) integrated CO emission. Contour levels are spaced at 0.1 K km s^{-1} intervals of 0.5 K km s^{-1} (black), and 0.2 K km s^{-1} intervals of 0.8 K km s^{-1} (white), respectively (from Yun & Clemens (1994), beam size of $48''$). A 5% polarization vector is drawn as reference for both data sets into the lower right corner. The well-ordered polarization pattern indicates dominant magnetic fields on scales of $10^3 - 10^6 \text{ au}$.

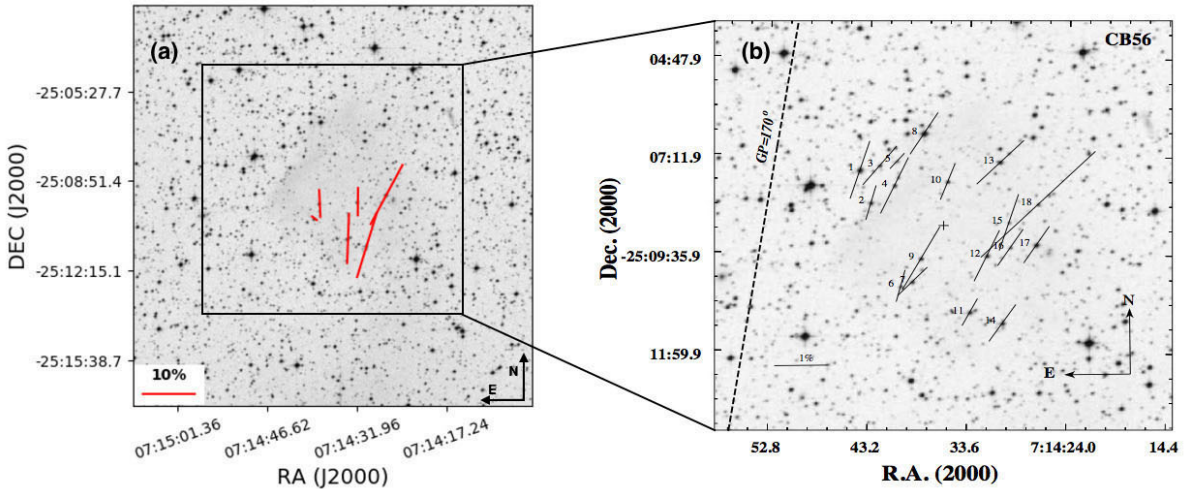


Fig. 2. (a) Near-IR polarization vectors plotted over a $15' \times 15'$ R-Band DSS image of the field containing CB56. A 10% polarization vector is drawn for reference in the lower left corner. Only the vectors with $P/\sigma_p \geq 3$ are plotted. (b) Optical polarization vectors of CB56, plotted over a $10' \times 10'$ R-Band DSS image (Chakraborty et al. 2014). A 1% polarization vector is drawn for reference in the lower left corner. The near-IR and optical polarization is strong and well-ordered, indicating dominant magnetic fields on scales of $10^4 - 10^5$.

For [OMK2002]18, archival data only in the sub-mm wavelength range were available (Matthews et al. 2009), in addition to the newly obtained near-IR polarization data. With these, an analysis of the polarization of the most dense center of the globule is possible (sub-mm), as well as an analysis of the less dense outer regions (near-IR).

In the following, we discuss the polarization maps separately, first focusing on the new near-IR data, and subsequently, comparing it to the maps of the optical and sub-mm wavelength ranges.

5.1. CB34

The polarization maps of the Bok globule CB34 are shown in Fig. 1. CB34 disclose a strong polarization signal, $P \geq 1\%$, in the outer, less dense regions observed in the near-IR (Fig. 4, Fig. 5). The polarization vectors in the near-IR wavelength range cover this Bok globule on scales of $10^4 - 10^5 \text{ au}$. The polarization structure in CB34 is well-ordered with a predominant North-West orientation.

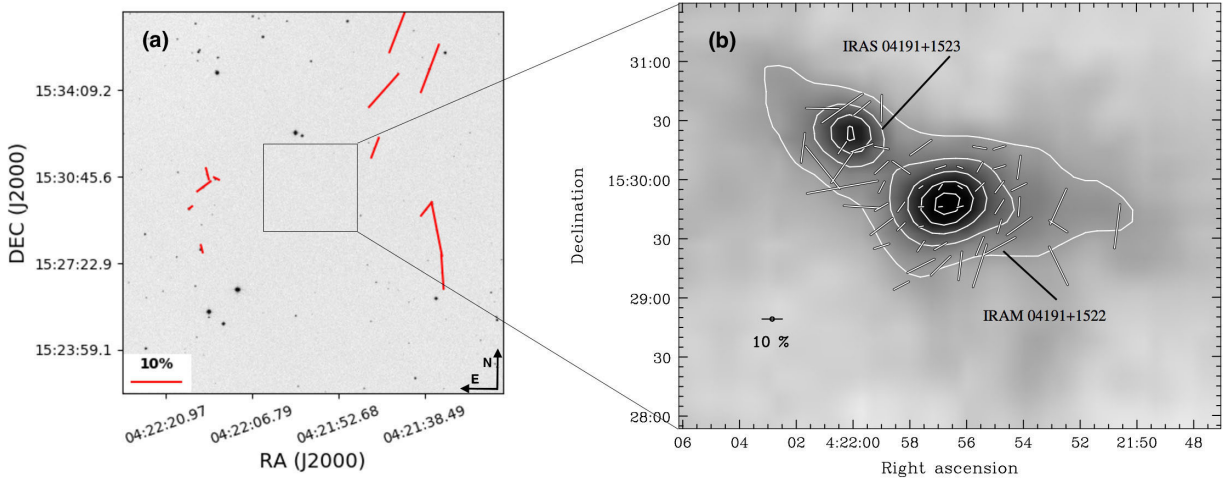


Fig. 3. (a) Near-IR polarization vectors plotted over a $\sim 20' \times 20'$ R-Band DSS image of the field containing [OMK2002]18. A 10% polarization vector is drawn for reference in the lower left corner. Only the vectors with $P/\sigma_p \geq 3$ were plotted. (b) Sub-mm polarization vectors of [OMK2002]18, plotted over a $20'' \times 20''$ grid. Contours correspond to JCMT/SCUBA $850 \mu\text{m}$ dust continuum emissions from 0.05 to $0.25 \text{ Jy beam}^{-1}$, with intervals of $0.05 \text{ Jy beam}^{-1}$ (Matthews et al. 2009, ©AAS. Reproduced with permission). Only Vectors with $P/\sigma_p \geq 2$ are plotted. The near-IR polarization is strong and well-ordered, indicating dominant magnetic fields on scales of $10^4 - 10^5 \text{ au}$ in the western region of the globule.

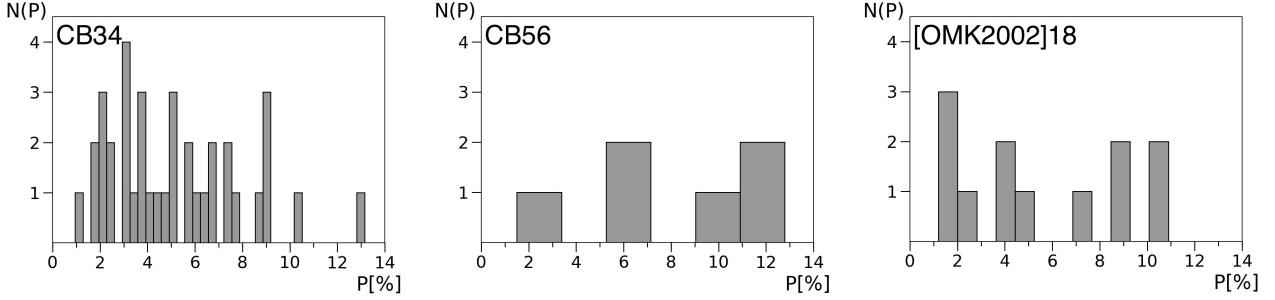


Fig. 4. Distribution of polarization degree, P for $P \geq 3\%$, counts given by $N(P)$, of CB34, CB56, and OMK[2002]18, observed in the near-IR.

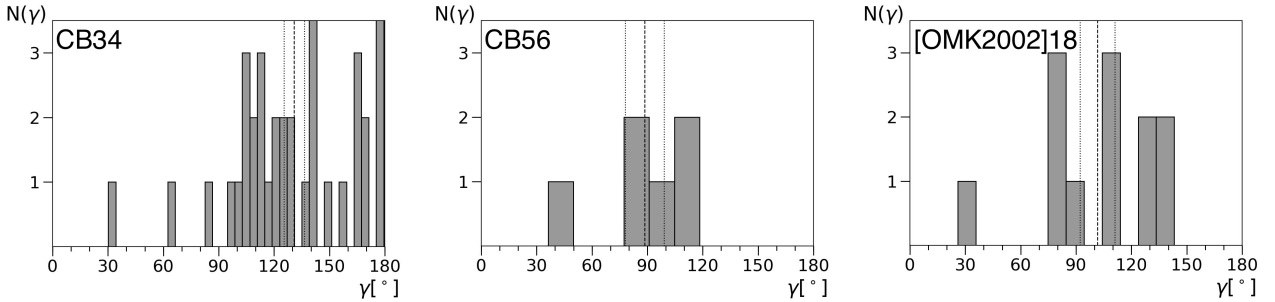


Fig. 5. Distribution of polarization angle, γ , counts given by $N(\gamma)$ of CB34, CB56, and OMK[2002]18, observed in the near-IR. The dashed lines represent the mean polarization angles, while dotted lines represent the corresponding 1σ deviation.

Most of the outer regions of this globule are traced in both near-IR and optical polarization. As expected from the wavelength dependency of polarization, we find stronger polarization degrees in the near-IR compared to the optical wavelength range. Both data sets fit well in orientation. The mean value of the polarization angle in the near-IR wavelength range in this regions is $\bar{\gamma}_{\text{near-IR}} \approx 134.3^\circ$, relatively consistent with the position angle of the galactic plane at the latitude of CB34, $\theta_{\text{GP}} \approx 148.7^\circ$. This suggests that the magnetic field is coupled to the Galactic magnetic field in the observed POS. This is similar to the findings from Das et al. (2016), based on the mean polarization angle in

the optical wavelength range. A more detailed analysis considering also the Planck results (Planck Collaboration et al. 2016) is beyond the scope of this study.

In the sub-mm, the polarization vectors can be associated to the cores C1 and C2, while there is no detection on top of C3 (Fig. 1). The region observed in the sub-mm overlaps with our near-IR data. The polarization vectors in the sub-mm wavelength range were plotted using the original data from Das et al. (2016). Thus, it has to be kept in mind that the vectors must be rotated 90° to be aligned with the magnetic field orientation. In this region, the orientation of the polarization vectors obtained in the

near-IR wavelength range fit very well to the sub-mm polarization vectors associated with core C1, but deviate stronger from those of core C2. Note that from the spatial distance between the near-IR and the sub-mm data on C2 it is not necessarily expected to have a direct correlation. In this region, the mean polarization angle in the near-IR wavelength is $\gamma_{\text{near-IR}} \approx 111.9^\circ$, which suggest that in this case the orientation of the magnetic field in the globule is different to the Galactic magnetic field. Similar findings were obtained in Das et al. (2016) using the data from the sub-mm wavelength range.

5.2. CB56

The polarization maps of the Bok Globule CB56 are shown in Fig. 2. CB56 discloses a strong polarization signal with polarization degrees of mostly 5% – 12% (Fig. 4). The polarization structure of this globule in the near-IR is well-ordered and predominantly oriented towards North-North/West (Fig. 5).

The region of CB56 which is covered by our near-IR observations overlays with the archival optical data set (Chakraborty et al. 2014). The polarization signal of the vectors measured from the optical wavelength range are weaker compared to the polarization vectors in the near-IR range, $P \approx 1\%$ for the very most of the optical polarization vectors. The polarization vectors obtained in both the optical and near-IR wavelength ranges are very well aligned within themselves, and fit well to each other. We find a slight deviation of the polarization orientation towards the dense center of the globules when switching from the optical to the near-IR wavelength range.

5.3. OMK[2002]18

The polarization maps of OMK[2002]18 is shown in Fig. 3. OMK[2002]18 shows a strong polarization signal, $2 \geq P \geq 10\%$, in all the regions observed in the near-IR (Fig. 4).

Two clearly divided regions of the globule can be observed in the near-IR wavelength range. The western region of the globule shows well-ordered polarization vectors in North-North/West orientation with strong polarization degrees of $P \approx 8\%$. The eastern region of the globule shows an unordered pattern with a much weaker polarization signal, $P \approx 2\%$ indicative for depolarization effects (e.g., Brauer et al. 2016). Considering the separation between these regions, uniformly ordered polarization vectors are not necessarily expected.

A spatial gap is seen between the sub-mm and near-IR polarization vectors, which of about 3.3×10^4 au. It originates in the sensitivity of SOFI/NTT, resp. SCUBA/JCMT (Bertrang et al. 2014). However, the near-IR polarization vectors in the western part of this object are well-aligned with the most external polarization vectors in the sub-mm wavelength range.

6. Magnetic Fields

In our analysis we assume that the magnetic field is oriented perpendicular to the measured polarization vectors in the sub-mm and parallel oriented to the measured polarization vectors in the near-IR and in the optical. This widely applied concept is based on the finding that, independently of the alignment mechanism, charged interstellar dust grains would have a substantial magnetic moment leading to a rapid precession of the grain angular momentum around the magnetic field direction, implying a net alignment of the grains with the magnetic field (e.g., Draine & Weingartner 1997; Lazarian 2007). However, one has to keep in

mind that polarization observations strongly suffer from projectional effects along the line-of-sight (LOS). Thus, for a comprehensive understanding of the magnetic field structure additional 3D radiative transfer modeling is essential but beyond the scope of this study.

In general, a high polarization signal is connected to a magnetic field strong enough to align the dust grains along the LOS. In Section 5, we find well-ordered polarization vectors on scales of 10^3 au to 10^5 au in all of the three Bok globules, CB34, CB56, and OMK[2002]18. This implies the presence of dominant large-scale magnetic fields in each globule.

In addition to this analysis, we can further estimate the magnetic field strength in the POS by using a method first proposed by Chandrasekhar & Fermi (1953) (CF method):

$$|B_{\text{POS}}| = \sqrt{\frac{4\pi}{3} \rho_{\text{gas}} \frac{v_{\text{turb}}}{\sigma_\gamma}}, \quad (1)$$

where ρ_{gas} is the gas density in units of g cm^{-3} , v_{turb} is the rms turbulence velocity in units of cm s^{-1} , and σ_γ the standard deviation of the polarization angles in radians. It is assumed that the magnetic field is frozen in the cloud material.

The total gas density, ρ_{gas} , is given by:

$$\rho_{\text{gas}} = 1.36 n_{\text{H}_2} M_{\text{H}_2}, \quad (2)$$

where $M_{\text{H}_2} = 2.0158$ amu is the mass of a H_2 molecule.

The rms turbulence velocity, v_{turb} , is given by (Wang et al. 1995):

$$v_{\text{turb}} = \frac{\Delta v}{2.35}, \quad (3)$$

where Δv is the FWHM line width, measured at quiescent positions located away from the emission peaks.

For CB34, the FWHM line width, Δv , is given by 1.5 km s^{-1} , and its mean density corresponds to $1.2 \times 10^4 \text{ cm}^{-3}$ in the region enclosing the star-forming cores C1 and C2 (Wang et al. 1995). For the outer, less dense regions, the mean density, n_{H_2} , is $3.76 \times 10^2 \text{ cm}^{-3}$ (Das et al. 2016) on average. With this we can estimate the mean magnetic field strength in several regions of CB34, namely the northern, the central, the southern, the eastern, and the western region of the globule. All parameters used for each region, including the derived magnetic field strength, are listed in Table 2.

In the outer part of CB34, traced by the near-IR and optical data set, we find similar magnetic field strengths of $B_{\text{CB34,near-IR,outer}} \approx (7 - 13) \mu\text{G}$ which are smaller than the magnetic field strengths derived from the sub-mm data ($B_{\text{CB34,sub-mm,C1}} \approx 34 \mu\text{G}$, $B_{\text{CB34,sub-mm,C2}} \approx 70 \mu\text{G}$; Das et al. 2016). In the central region of CB34, the near-IR data traces the magnetic field associated with the core C1 (Fig. 1). The magnetic field strength derived from the near-IR data ($B_{\text{CB34,near-IR,center}} \approx 360 \mu\text{G}$), is stronger than those traced in the sub-mm wavelength range. However, considering the inaccuracies in the estimations of the densities, the temperatures, and the gas velocities, we do not find any significant difference in the magnetic field strengths in the inner and outer parts of CB34.

For CB56 and OMK[2002]18, information on the gas densities and turbulence velocities in the regions traced in the presented polarization data is not available.

Table 2. Gas densities, gas velocities, polarization, and magnetic field strengths of the regions of CB34 traced in the near-IR.

Region	n_{H_2} (cm^{-3})	ρ_{gas} (g cm^{-3})	Δv (km s^{-1})	v_{turb} (km s^{-1})	N_{vec}	$\bar{\gamma}$ (rad)	σ_{γ} (rad)	B (μG)
North	3.76×10^2	1.71×10^{-21}	1.5	0.64	7	2.055	0.728	7.442
South	3.76×10^2	1.71×10^{-21}	1.5	0.64	6	1.999	0.531	10.204
East	3.76×10^2	1.71×10^{-21}	1.5	0.64	9	2.591	0.418	12.963
West	3.76×10^2	1.71×10^{-21}	1.5	0.64	10	2.504	0.551	9.833
Central	1.2×10^4	5.46×10^{-20}	1.5	0.64	5	1.954	0.200	358.675

References. (1) Whittet et al. (1992); (2) Turnshek et al. (1990); (3) Fossati et al. (2007).

7. Correlation between magnetic field structure and the CO outflow

Alongside the collapse of the dust in Bok globules, magnetic fields are also presumed to influence the formation of circumstellar disks and outflows (e.g., Matsumoto et al. 2006; Bertrang et al. 2017; Bertrang & Wolf 2017). Both aligned and misaligned orientation of the outflow axes along the magnetic field directions have been reported (e.g., Jones & Amini 2003; Bertrang et al. 2014). Based on MHD simulations, Matsumoto et al. (2006) find that the alignment degree between outflow and magnetic field is directly correlated to the magnetic field strength: the stronger the magnetic field, the better the alignment. In the following, we examine the relative position of the outflow axes and the magnetic field directions for the inner, most dense part of CB34, using our data in the near-IR wavelength range as well as the archival data in the optical and sub-mm wavelength range.

In discussing the relative orientation between the CO outflow and the magnetic field, one has to consider that only one component of the spatial orientation of the outflow ($v \sin i$) is known from velocity measurements, so projectional effects have to be considered, as well as that polarization vectors only trace the magnetic field structure projected on the plane of sky. We assume that the magnetic field is oriented parallel to the polarization vectors in the near-IR wavelength range, and perpendicular to the polarization vectors in the sub-mm wavelength range.

The orientation of the CO outflow of CB34 is roughly parallel to the axis linking the cores C1 and C2 (Khanzadyan et al. 2002), indicating a North-East to South-West orientation. The orientation of polarization vectors in the near-IR and optical wavelength range, tracing the less-dense outer part of the globule, is almost perpendicular to the direction of the outflow. However, the polarization vectors in the sub-mm polarization range, tracing the dense center of the globule, are roughly aligned to the outflow direction, especially for those related to core C1.

The comparison between orientation of the polarization vectors in this globule in the optical, near-IR, and sub-mm wavelength ranges to the CO outflow suggests that there is a correlation between the magnetic field orientation and the direction of the outflow, depending on the density and distance to the protostellar core.

8. Conclusions

For the first time, we have obtained near-IR polarization data and, in conjunction with archival optical and sub-mm data, compiled multi-wavelength polarization maps which allow for the verification of the magnetic field influence on scales of $10^3 - 10^6$ au in the Bok globules CB34, CB56, and [OMK2002]18, covering optically thin and optically thick regions. The major results are:

1. We find a strong polarization signal of several percents in all three Bok globules in the near-IR.
2. In CB34, the polarization vectors in the near-IR are well aligned with those obtained in the optical tracing scales of $10^5 - 10^6$ au as well as with those obtained in the sub-mm which trace the innermost, densest part of the globule on scales of 10^3 au.
3. In CB56, the polarization vectors in the near-IR are well-aligned with those obtained in the optical wavelength range on scales of $10^4 - 10^5$.
4. In [OMK2002]18, the polarization vectors in the western region are well-ordered and show high polarization degrees, while we find indications for depolarizing effects in the eastern region.
5. We find a correlation between the magnetic field structure and the CO outflow of the Bok globule CB34, depending on the density and distance to the protostellar core.
6. For CB34, comparable magnetic field strengths are found in the regions traced in the near-IR resp. sub-mm observations by applying the CF method.
7. Our findings determine the distance of CB56 to ≤ 200 au, for the first time.

In the case of CB34, the ordered polarization vectors indicate the presence of dominant magnetic fields in scales of $10^3 - 10^4$ au and $10^5 - 10^6$ au. The sub-mm data shows polarization vectors in a East-West orientation in the central regions of the globule (core C2) that changes to a North-South orientation in external parts (core C1). On scales of $10^4 - 10^6$ au the orientation of the polarization vectors in the near-IR and optical wavelength range change slightly towards an East-West orientation, potentially coupling with the Galactic magnetic field. This indicates that only the magnetic fields in the inner, most dense regions of the globule are related to the gravitational collapse of the globule, while the magnetic fields of the outer regions are dominated by the Galactic magnetic field. The scale of the transition is $\sim 10^4$ au.

In the case of CB56, the ordered polarization vectors and high polarization degrees in the optical and near-IR wavelength ranges indicate the presence of a dominant magnetic field in the observed regions on scales of $10^4 - 10^5$ au.

In the case of [OMK2002]18, due to the gap separating the regions observed in the near-IR and sub-mm wavelength ranges, it is not possible to spatially connect the magnetic field observations from the inner to the outer regions. Furthermore, as stated in Section 5, the eastern region of the globule exhibits evidence of depolarization effects. However, when considering the western region of the globule, the polarization vectors in the near-IR and sub-mm wavelength range trace a strong and well-ordered polarization signal, indicative for dominant magnetic fields on scales of $10^4 - 10^5$ au.

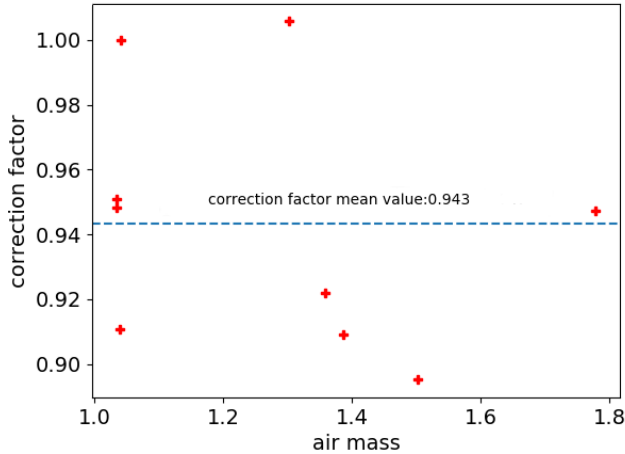


Fig. A.1. Comparison between the correction factor that minimizes the instrumental polarization and the air mass of the observed unpolarized standard stars. The dashed line correspond to the mean value of the computed correction factors. Unlike for ISAAC/VLT (Bertrang et al. 2014), we do not find a correlation between the instrumental polarization and the elevation angle of the telescope, resp. the airmass of the object.

Appendix A: Correction factor derivation for Wollaston prism

As stated in Section 4, a correction factor, C_λ for the Wollaston prism has to be calculated to correct for the instrumental polarization, as the transmission ratio of the prism is not ideal. This correction factor is applied to the intensities of the upper, i_u , and lower, i_l , beams created by the Wollaston prism in the following way:

$$\begin{aligned} i_{u,2} &= i_{u,2} * C_\lambda \\ i_{l,2} &= i_{l,1} \end{aligned} \quad (\text{A.1})$$

In our previous study, we find that the instrumental polarization for an instrument in Nasmyth focus has a strong dependency of the elevation angle of the telescope (ISAAC/VLT; Bertrang et al. 2014). For the here presented study, we test SOFI/NTT for this dependency as well. To determine the instrumental polarization, C_λ has to be adjusted in such a way that the measured polarization of the unpolarized standard star is minimal.

From November 11 to November 15, 2015, we observed unpolarized standard stars (see Tab. 1) and derive C_λ dependent on the elevation angle of the telescope, resp. the airmass of the object (see Fig. A.1). We find no correlation between the correction factor, C_λ , and the elevation angle of SOFI/NTT. Hence, we use the mean value of the correction factor to reduce our data. Please note that we observed several standard stars with SOFI/NTT over only a few nights. Observations of the same target over a longer period, as performed in Bertrang et al. (2014), might result in a different finding.

Acknowledgements. We thank Amelia M. Stutz for informative and helpful discussions. GHMB acknowledges financial support from CONICYT through FONDECYT grant 3170657.

References

- Alves, J., Hartmann, L., Briceno, C., & Lada, C. J. 1997, *AJ*, 113, 1395
Bertrang, G., Wolf, S., & Das, H. S. 2014, *A&A*, 565, A94

- Bertrang, G. H. M., Flock, M., & Wolf, S. 2017, *Monthly Notices of the Royal Astronomical Society: Letters*, 464, L61
Bertrang, G. H.-M. & Wolf, S. 2017, *MNRAS*, 469, 2869
Bok, B. J. & Reilly, E. F. 1947, *ApJ*, 105, 255
Brauer, R., Wolf, S., & Reissl, S. 2016, *Astronomy & Astrophysics*, 588, A129
Chakraborty, A. & Das, H. S. 2016, *Ap&SS*, 361, 321
Chakraborty, A., Das, H. S., & Paul, D. 2014, *MNRAS*, 442, 479
Chandrasekhar, S. & Fermi, E. 1953, *ApJ*, 118, 113
Clemens, D. P. & Barvainis, R. 1988, *ApJS*, 68, 257
Clemens, D. P., Yun, J. L., & Heyer, M. H. 1991, *ApJS*, 75, 877
Codella, C. & Scappini, F. 2003, *MNRAS*, 344, 1257
Das, A., Das, H. S., Medhi, B. J., & Wolf, S. 2016, *Ap&SS*, 361, 381
Draine, B. T. & Weingartner, J. C. 1997, *The Astrophysical Journal*, 480, 633
Dutra, C. M. & Bica, E. 2002, *A&A*, 383, 631
Federrath, C. 2015, *MNRAS*, 450, 4035
Fossati, L., Bagnulo, S., Mason, E., & Landi Degl'Innocenti, E. 2007, in *Astronomical Society of the Pacific Conference Series*, Vol. 364, *The Future of Photometric, Spectrophotometric and Polarimetric Standardization*, ed. C. Sterken, 503
Galli, D. 2009, *Mem. Soc. Astron. Italiana*, 80, 54
Girart, J. M., Rao, R., & Marrone, D. P. 2008, *Ap&SS*, 313, 87
Gómez, J. F., de Gregorio-Monsalvo, I., Suárez, O., & Kuiper, T. B. H. 2006, *AJ*, 132, 1322
Henning, T., Wolf, S., Launhardt, R., & Waters, R. 2001, *ApJ*, 561, 871
Hoang, T., Lazarian, A., & Yan, H. 2007, in *Bulletin of the American Astronomical Society*, Vol. 39, *American Astronomical Society Meeting Abstracts*, 984
Huard, T. L., Weintraub, D. A., & Sandell, G. 2000, *A&A*, 362, 635
Jones, T. J. & Amini, H. 2003, *AJ*, 125, 1418
Khanzadyan, T., Smith, M. D., Gredel, R., Stanke, T., & Davis, C. J. 2002, *A&A*, 383, 502
Launhardt, R., Evans, II, N. J., Wang, Y., et al. 1998, *ApJS*, 119, 59
Launhardt, R. & Henning, T. 1997, *A&A*, 326, 329
Launhardt, R., Nutter, D., Ward-Thompson, D., et al. 2010, *ApJS*, 188, 139
Lazarian, A. 2007, *J. Quant. Spectr. Rad. Transf.*, 106, 225
Lizano, S. & Galli, D. 2015, in *Astrophysics and Space Science Library*, Vol. 407, *Magnetic Fields in Diffuse Media*, ed. A. Lazarian, E. M. de Gouveia Dal Pino, & C. Melioli, 459
Maheswar, G., Lee, C. W., & Dib, S. 2011, *A&A*, 536, A99
Matsumoto, T., Nakazato, T., & Tomisaka, K. 2006, *ApJ*, 637, L105
Matthews, B. C., McPhee, C. A., Fissel, L. M., & Curran, R. L. 2009, *ApJS*, 182, 143
McKee, C. F. & Ostriker, E. C. 2007, *ARA&A*, 45, 565
Onishi, T., Mizuno, A., Kawamura, A., Tachihara, K., & Fukui, Y. 2002, *ApJ*, 575, 950
Paul, D., Das, H. S., & Sen, K. 2012, *Bulletin of the Astronomical Society of India*, 40, 113
Planck Collaboration, Ade, P. A. R., Aghanim, N., et al. 2016, *A&A*, 594, A19
Turnshek, D. A., Bohlin, R. C., Williamson, II, R. L., et al. 1990, *AJ*, 99, 1243
Wang, Y., Evans, II, N. J., Zhou, S., & Clemens, D. P. 1995, *ApJ*, 454, 217
Weintraub, D. A., Goodman, A. A., & Akeson, R. L. 2000, *Protostars and Planets IV*, 247
Whittet, D. C. B., Martin, P. G., Hough, J. H., et al. 1992, *ApJ*, 386, 562
Yun, J. L. & Clemens, D. P. 1994, *ApJS*, 92, 145